Eur Biophys J (1994) 23:39–49

European Biophysics Journal

Implication of segment S45 in the permeation pathway of voltage-dependent sodium channels

M. Brullemans, O. Helluin, J.-Y. Dugast, G. Molle, H. Duclohier

URA 500 CNRS, Université de Rouen, Boulevard Maurice de Broglie, F-76821 Mont-Saint-Aignan Cedex, France

Received: 7 July 1993 / Accepted in revised form: 3 November 1993

Abstract. A 34-mer peptide, encompassing the S4 and S45 segments of domain IV of the electric eel voltage-dependent sodium channel, was synthesized in order to test the potential implication of S45 in the gating or permeation pathway. The secondary structure of peptide S4-S45 assessed by circular dichroism was found mainly helical, both in organic solvents and in lipid vesicles, especially negatively-charged ones. The macroscopic conductance properties of neutral and negatively-charged Montal-Mueller planar lipid bilayers doped with S4-S45 were studied and compared with those of S4. With regard to voltage-dependence, the most efficient system was S4-S45 in neutral bilayers. Voltage thresholds for exponential conductance development were found to correlate with the background or "leak" conductance. Assuming that the latter reflects interfacial peptide concentration, the mean apparent number of monomers per conducting aggregate could be estimated to be 3–5. In single-channel experiments, the most probable events had amplitudes of 8 pS and 5 pS in neutral and negatively-charged bilayers respectively. Ionic selectivity under salt gradients conditions, both at macroscopic and single-channel levels, was in favour of sodium ions ($P_{Na}/P_K = 3$). These properties compare favourably to previous reports dealing with peptide modelling transmembrane segments of voltage-dependent ionic channels. Specifically, when compared to S4 alone, the reduced unit conductance and the increased selectivity for sodium support the implication of the S45 region in the inner lining of the open configuration of sodium channels.

Key words: Voltage-dependent sodium channels – Synthetic model peptides – Voltage-gating – Ion selectivity – Planar lipid bilayers

Correspondence to: H. Duclohier

Introduction

Transient changes in membrane ion permeability mediating electrical signal generation and propagation in excitable cells are initiated by voltage-dependent ionic channels. The rapid rising phase of action potentials corresponds to the opening (or activation) of voltage-dependent sodium channels whose subsequent inactivation is partly responsible for membrane repolarisation. Relaying purification and reconstitution studies, the elucidation of the primary structure of voltage-gated ionic channels provided the impetus for topological models as well as electrophysiological tests of channels subjected to site-directed mutagenesis and expressed in oocytes through cDNA injection.

Nearly all members of the voltage-dependent channels superfamily share the same general architecture: the main α-subunit is composed of one or four homologous domains, each of which consists of six transmembrane segments, S1 to S6. At the risk of oversimplification, two regions are assumed to be functionally important: SS1–SS2 (or P-region or H5) would line the pore and govern its selectivity (Yool and Schwarz 1991) while S4, characterized by positively charged residues at every third position, is recognized by site-directed mutagenesis as the main voltage-sensor, responsible for the gating (Stühmer et al. 1989).

Evidence from gating current kinetics in the squid giant axon (Keynes et al. 1990) suggests two steps for the movement of each S4, which must not be regarded as strictly identical in all four domains (Patlak 1991). In particular, S4 from domain IV being the most heavily charged, is assumed to play a role in inactivation as well (Keynes 1992). For all events, only the first activation step would be voltage-dependent and there is now good evidence (effects of H_2O/D_2O replacement or hyperosmolar media) that the second step would be rather solvent-sensitive (Schauf and Bullock 1980; Rayner et al. 1992). It has to be recognized that the concerted outward movement (about 10 Å) of S4 segments visualized as in the "helical screw" hypothesis (Catterall 1986) would have profound

consequences on the contiguous segments and connecting loops. As an alternative to the above-mentioned mechanism, a "propagating helix" model (Guy and Conti 1990) was proposed to account for the channel activation. According to this model, S4 segments line the pore and upon depolarisation undergo secondary structure changes. More recently, Durell and Guy (1992) extended the helical screw hypothesis by proposing that the C-contiguous segment, S45, could play a role in the gating (specifically in the solvent-sensitive step) as well as forming the inner part of the pore lining. Experimentally, mutations in the S4–S5 linker of potassium channels affect the single-channel conductance (Slesinger et al. 1993) and shift activation-voltage curves (Smith-Maxwell et al. 1993). Besides, this S4–S5 linker (equivalent to S45) is assumed to form part of the receptor for the inactivation gate and to lie near the pore exit (Isacoff et al 1991).

Another and complementary approach, advocated in Stühmer's review (1991), makes use of synthetic channel-forming peptides (Spach et al. 1989; Sansom 1991). This stems from pioneering studies on alamethicin conferring excitability properties, when used in conjunction with basic polypeptides rich in arginines, such as S4, to artificial membranes (Mueller and Rudin 1968). Later extended with the "barrel-stave" model, i.e. aggregates of amphipathic peptide monomers (Baumann and Mueller 1974), this approach now takes advantage of first principles of peptide chemistry to design ion channels models (Lear et al. 1988). Attempts to dissect out aspects of structure-function for various channels include the sodium channel S3 (Oiki et al. 1988 b) and S4 (Tosteson et al. 1989) segments, the M2 helices of the nicotinic acetylcholine and glycine receptors (Oiki et al. 1988 a; Langosch et al. 1991), and also a transmembrane segment of the mitochondrial H^+ ATP synthetase (Molle et al. 1988). More recently, the method was applied to the putative transmembrane segment of the minK potassium channel (Ben-Efraim et al. 1993).

In order to test the eventual involvement of S45 in sodium channel function, we have synthesized a 34-mer peptide encompassing S4 and S45 regions of domain IV (positions 1 414 to 1 447) from the electric eel sodium channel sequence (Noda et al. 1984). Its macroscopic and single-channel conductance properties in neutral and negatively-charged planar lipid bilayers were investigated and compared with those of S4 alone, previously studied by Tosteson et al. (1989), who kindly provided a sample.

Segment S4–S45 (domain IV):

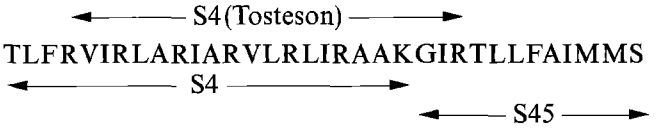

Materials and methods

Solid-phase peptide synthesis

S4–S45 peptide was prepared by the solid-phase technique (Merrifield 1963) on a SAP 4 synthesizer model from Sempa-Chimie (Paris). Briefly, t-Boc-serine was coupled to the benzhydrylamino resin reticulated by 1% divinylbenzene. The synthesis proceeded stepwise towards the N-terminus using 1-hydroxybenzotriazole (HOBt) and N–N′-dicyclohexylcarbodiimide (DCC) as coupling co-reagents. To avoid oxidization hazards during the subsequent purification, the two Met residues near the C-terminus were replaced by *nor*-Leu. After each step, a ninhydrin test allowed the estimation of the coupling yield. Some coupling steps had to be repeated and acetylation was used to block the remaining free amino groups. Providing a negative ninhydrin test, the amine function was deprotected with trifluoroacetic acid (TFA) (30% in CH_2Cl_2) and the peptide resin was neutralized by diisopropylethylamine (DIEA) (10% in CH_2Cl_2) before coupling the following amino acid. After completion of the synthesis and acetylation of the N-terminus, the peptide was released from the resin and side chain protecting groups eliminated by the usual fluorohydric acid treatment.

HPLC purification, FAB mass characterization and circular dichroism

The lyophilized raw product was purified by HPLC (LKB System, series 2 100, Pharmacia LKB Biotechnology, Bromma, Sweden) through repeated steps on a reverse phase semi-preparative column (C_{18}, 10 µm, 8 × 300mm), from Société Française Chromato Colonne/Shandon Scientific (Eragny, France) under acetonitrile/H_2O gradients.

Electro-spray and Fast Atomic Bombardment (FAB) positive ion mass spectrometries allowing an unambiguous characterization of the purified peptide were carried out at the laboratory of mass spectrometry of Strasbourg (Centre de Neurochimie, Université Louis Pasteur) and at the Service Central d'Analyses du CNRS (Solaize, France), respectively.

Circular dichroism spectra of the peptide S4–S45 in methanol (spectroscopic grade, Sigma) and in trifluoroethanol (for synthesis, Merck) solutions were recorded at 1 mg/mL on a spectropolarimeter (Dichrograph Mark V, Jobin-Yvon, Longjumeau, France) using a 0.1 mm quartz cell. CD was also performed with lipid SUV (Small Unilamellar Vesicles) suspensions in 100 mM NaCl, 2 mM HEPES, pH 7.4. Either neutral (egg lecithin from Sigma, product number 2772) or anionic (egg PC/POPS, 1/1, w/w) SUVs at 1 mM lipid concentration were prepared by sonication. A "blank" spectrum was thus recorded (to be substracted) and the peptide was added from a buffer solution to yield a final concentration of 0.2 mg/mL. Several scans between 190 and 250 nm were averaged and the different conformational contents estimated from 51 molar ellipticity values (from 190 to 240 nm, every nanometer). The standards we used were based on fifteen proteins (Chang et al. 1978).

Peptide reconstitution into planar lipid bilayers

In macroscopic conductance experiments, virtually solvent-free lipid bilayers were formed over a 125 µm hole in

a 25 μm thick PTFE (Goodfellow, Cambridge, UK) septum sandwiched between two half glass cells. Lipid films were spread on top of electrolyte solutions (500 mM NaCl, 10 mM HEPES, pH 7.4) in both compartments and bilayer formation was most often achieved by lowering and then raising the level in one or both sides (Montal and Mueller 1972). The lipid solution at 1–5 mg/mL in hexane (Fluka, spectroscopic grade) was either a neutral mixture: 1-palmitoyl, 2-oleoyl phosphatidylcholine (POPC)/1,2-dioleoylphosphatidylethanolamine (DOPE), 7/3 (w/w), or a negatively-charged one: 1-palmitoyl, 2-oleoyl phosphatidylserine (POPS)/1,2-dioleoyl phosphatidylethanolamine, 1/1 (w/w). These mixtures are simply referred to as PC–PE and PS–PE hereafter. These lipids were purchased from Avanti Polar Lipids (Alabaster, AL, USA) and stored at −74 °C. Voltage was applied through an Ag/AgCl electrode in the cis (or positive) side to which the peptide (from a 10^{-5} M stock solution in acetonitrile/H_2O, 1/1, v/v) was added with stirring. Transmembrane currents were fed to a Keithley amplifier (model 427, Cleveland, Ohio, USA) virtually grounded to the trans Ag/AgCl electrode. Current-voltage curves were recorded from an X-Y plotter (model LY1600, Linseis, Selb, Germany).

In single-channel experiments, lipid bilayers were formed at the tip of fire-polished patch-clamp pipettes pulled in two steps (model PP-83, Narishige, Tokyo, Japan) from Vitrex borosilicate tubes (Modulohm, Herlev, DK). From the "bubble number" of the pipette in methanol and its resistance (≈ 5 MΩ) in the standard electrolyte solution described above, the tip diameter could be estimated to be 0.6–1.0 μm. The same neutral and negatively-charged lipid mixtures, as in the macroscopic conductance configuration but at 0.1 or 0.5 mg/mL in hexane, were allowed to evaporate on top of 2 mL of the electrolyte solution in a glass beaker (spreading area: 3 cm^2). To form bilayers, either the pipette was withdrawn and then slowly dipped again (by means of a hydraulic micromanipulator, model 468M, L. S. Starrett Ltd, UK) or a lipid droplet was applied to the pipette shank (Hanke et al. 1984). A programmable waveform generator (SMP 310 model) and a patch-clamp amplifier (RK-300) both from Bio-Logic (Claix, France) were used to record single-channel currents. The latter were fed to an 8 pole Bessel filter and stored on a digital tape recorder (respectively, AF 180 and DTR 1200 models from Bio-Logic). Analog to digital conversion and numeric signals analysis were subsequently performed through the S200 interface and Satori program v. 3.01 from Intracel Ltd (Royston, UK). Nonlinear least-squares fitting of raw data was made through the software packages NFIT (Island Products, Galveston, Tex, USA) and ASYSTANT (Asyst Software Technologies Inc., Rochester, NY, USA).

Results

Synthesis, purification and characterization of peptide S4–S45

The solid-phase technique with a benzhydrylamino resin (5 g with a substitution coefficient of 0.6 mmol of amino-sites per gram of resin) was used to synthesize peptide S4–S45. For each coupling step, 1.5 milliequivalents of each reactant (protected amino acid, DCC, HOBt) were used. The N-terminus was acetylated and the HF treatment of the peptidyl-resin (final mass: 1 115 mg) left an amidated C-terminus. The lyophilized raw product (460 mg) was pre-purified on reverse phase column under an acetonitrile/H_2O gradient. Owing to the presence of a contaminant, revealed by electrospray analysis, another preparative HPLC step was needed to yield the final product whose purity was greater than 98%. FAB mass spectroscopy showed a molecular mass (3 945.9 mass units) agreeing, within two mass units on accounting for the statistical abundance of the C^{13} isotope, with the theoretical one (3 943.5). As the examination of the fragment masses (mainly A-type ions) and Edman sequencing confirmed the expected sequence up to isoleucine 24, there remains no doubt as to the generated sequence.

Circular dichroism spectroscopy of the peptie S4–S45 in various media was performed in order to assess the proportions of different conformations (helical, β-sheet, β-turn and random coil). Results, summarized in Table 1, are from a constrained method of analysis i.e. the sum of the four conformations was set to 100%. The normalized mean root square deviation (last column) is an index of the quality of the fit of calculated spectra to the experimental ones. Values obtained from unconstrained least-squares algorithm were not significantly altered, especially as regards the helical contribution which remained predominant in all systems, except maybe for neutral vesicles. Note the increased helicity and β-content of S4–S45 in negatively-charged lipid vesicles at the expense of random coil conformation.

Table 1. Calculated secondary structure of segment S4–S45 from CD measurements

Medium	*H*(%)	*B*(%)	*T*(%)	*R*(%)	NMRSD(%)
Methanol	50	21	0	29	12.5
Trifluoroethanol	48	13	0	39	15.1
PC SUV	37	17	7	39	15.0
PC-PS (1:1) SUV	54	32	4	10	21.5

SUV: Small Unilamellar Vesicles; *H*, *B*, *T* and *R*: proportion of helical, β-sheet, β-turn and random coil conformations; NMRSD: normalized root mean square deviation (Brahms and Brahms 1980)

Macroscopic conductance studies

The conductance properties induced by S4–S45 in lipid bilayers were investigated in the first instance at the macroscopic conductance level in Montal-Mueller bilayers of relatively large area doped with the order of a thousand channels. In principle, with this configuration, voltage and concentration dependences can be readily obtained.

Voltage-dependence of macroscopic currents and conductances. Figure 1 A depicts a typical recording of current-voltage relations when the bilayer, submitted to a trian-

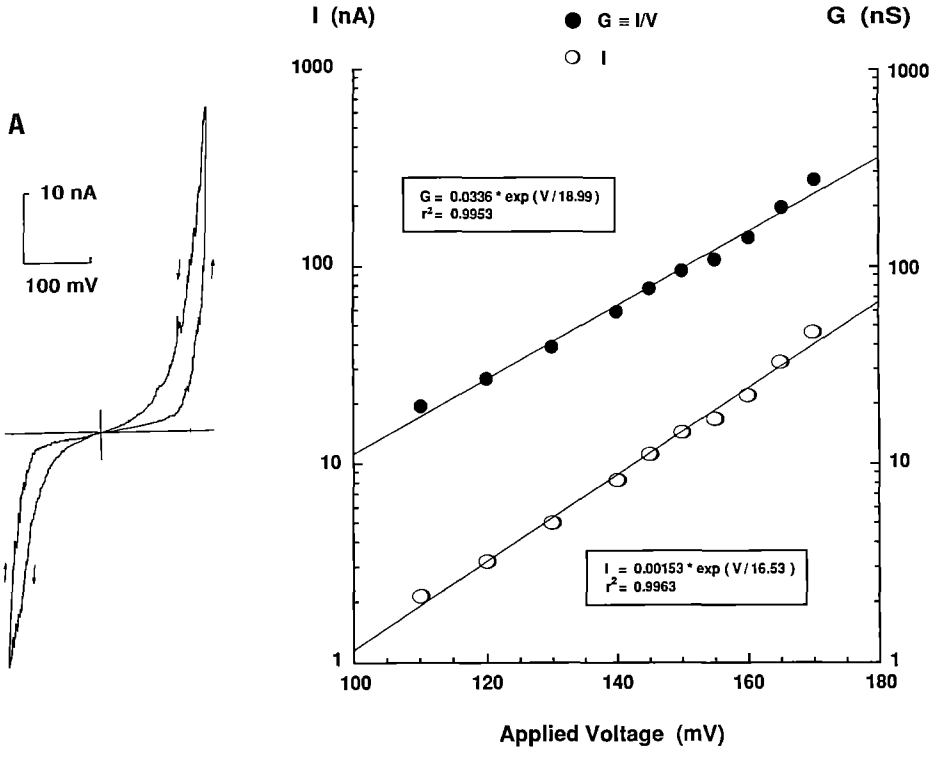

Fig. 1. A Macroscopic current-voltage curve for peptide S4–S45 at a bath (cis) concentration of 100 nM. Lipids: POPC-DOPE (7:3). Aqueous phases: 500 mM NaCl, 10 mM HEPES, pH 7.4. Hole diameter: 150 μm. The bilayer was submitted to a voltage ramp at 15 mV s^{-1}. The slope conductance at low voltage (ascending branch) was 12 nS. **B** Semilog plot of current and conductance vs voltage for the experimental I–V curve shown on part A (ascending branch). Expression for best fits and the related correlation coefficient appear in the inserts. The ohmic region is not represented

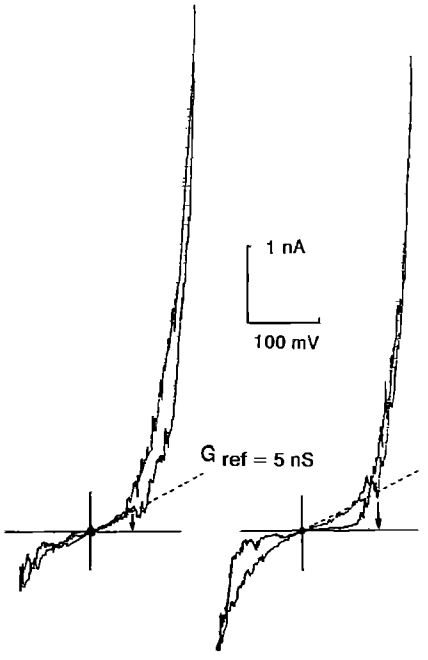

Fig. 2. Two macroscopic I–V curves from a POPS-DOPE (1:1) bilayer recorded within an interval of 8 min. The aqueous concentration of the S4–S45 peptide in the cis side was 200 nM. Aqueous phases: 500 mM NaCl, 10 mM HEPES, pH 7.4. Hole diameter: 125 μm. Note the displacement of the characteristic voltage (defined as the positive voltage of the ascending branch corresponding to a reference conductance (here 5 nS) with the conductance near zero current, $G(0)$

gular voltage waveform, was equilibrated ($t = 20$ min) with 100 nM aqueous concentration of S4–S45 in the cis side. The current response appears symmetrical with respect to zero-voltage and above a threshold develops rapidly upon the backgrounded or leak conductance. The leak conductance was defined here as the slope of I–V curves near zero-current and was referred to hereafter as $G(0)$. Note that, contrasting with the alamethicin case for example, ascending and descending limbs cross at 0 mV such that hystereses are reversed according to the voltage polarity. The rise of membrane current in this example is analysed in Fig. 1 B, showing an exponential dependence of current and conductance. V_e' and V_e, voltage increments resulting in e-fold changes in current and conductance, are 16.5 and 19.0 mV respectively. These values were determined by nonlinear regression. As shown by correlation coefficients, the non-ohmic part can be fitted either by the relation $I \propto V \cdot \exp(V/V_e)$ or by $I \propto \exp(V/V_e')$. Ten other I–V curves obtained in the two lipid mixtures were analysed and values for the steepness parameters determined.

During the course of successive I–V runs, $G(0)$ and the rate of exponential development of current or conductance were found to be somewhat variable (see for example Fig. 2). This situation is reminiscent of the one reported for DOPC bilayers doped with mellitin (Pawlak et al. 1991). However, as shown by Fig. 3, V_e was correlated with $\log G(0)$ in the four systems studied, i.e. S4–S45 compared to S4 alone either in neutral or in negatively-charged bilayers. In terms of voltage-sensitivity, the most efficient system seems to be S4–S45 in PC–PE membranes ($V_e = 9$ to 19 mV).

"Concentration-dependence" of macroscopic currents and conductances. Whatever the lipids used for the bilayers, no obvious correlation could be found when characteristic voltages, i.e. thresholds at which conductances attained a reference value (5 nS for example, Fig. 2), were plotted vs S4–S45 concentration in the bath. This variability could be a consequence of the lack of control on

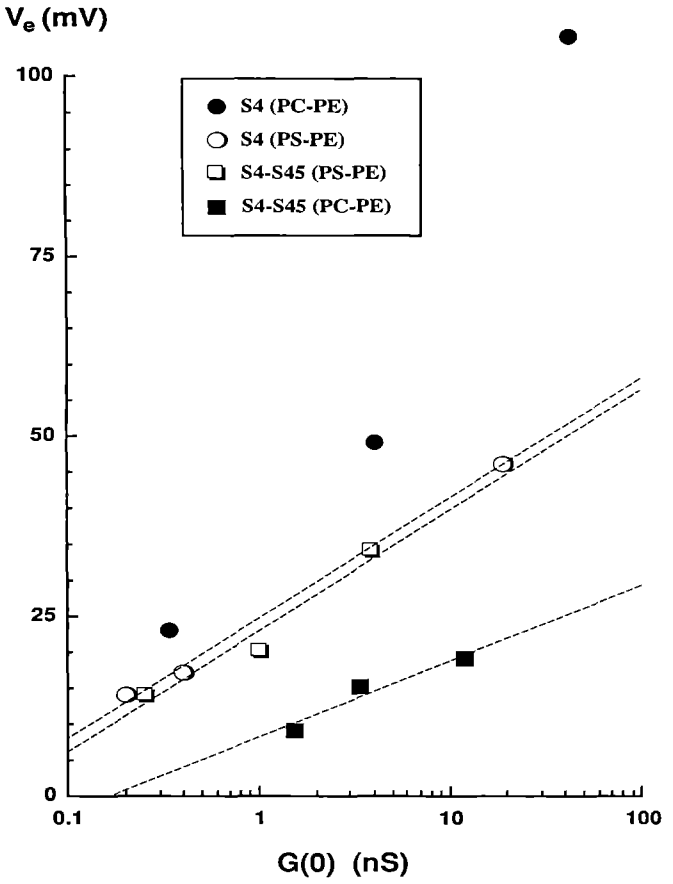

Fig. 3. Semi-log plot of steepness parameter V_e vs $G(0)$. V_e values are determined by nonlinear least-squares fitting, as in Fig. 1 B, and $G(0)$ from enlarged I–V curves

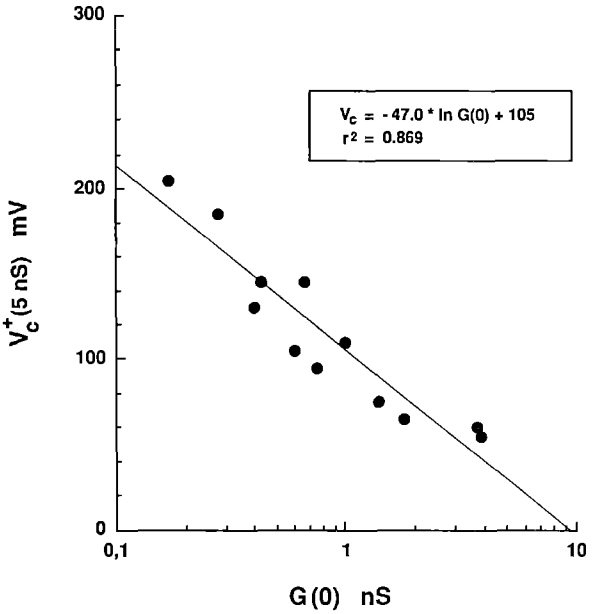

Fig. 4. Graph of V_c (5 nS) versus the logarithm of $G(0)$ for POPS-DOPE (1:1) bilayers. Each point represents a different I–V curve usually recorded from different bilayers. The slope of the regression line gives the parameter V_b, here −47 mV

diffusion, adsorption and aggregation of this peptide in aqueous solutions, but also of the particular conditions prevailing during the bilayer formation, which could alter its subsequent properties (Brullemans and Tancrède 1987). On the other hand, if characteristic voltages V_c were plotted as a function of $\log G(0)$ once more, a linear decrease was obtained for all systems. For the case of S4–S45 in PS-PE bilayers, the correlation coefficient increased from 0.038 when nominal bath concentrations were taken into account to 0.869 with $\log G(0)$ as illustrated in Fig. 4. V_b, the V_c shift for an e-fold change in $G(0)$ was here -47 ± 6 mV. The same treatment for the three other systems (S4–S45 in PC-PE, S4 in PS-PE, S4 in PC-PE) yielded respectively: -37 ± 6, -46 ± 11 and -35 ± 5 mV. The number of analysed I–V curves varied between 6 and 19.

Sizes of the conducting aggregates and apparent gating charge. If we assume that the ohmic background conductance $G(0)$ reflects the intrinsic membraneous peptide concentration locked into voltage-insensitive conducting aggregates until a voltage threshold is reached, the formalism derived by Hall et al. (1984) for alamethicin can be adapted by using for V_a the V_b shift defined above. Given the fact that the number of conducting aggregates is more directly related to the peptide concentration in the bilayer than the one in the bath, this substitution seems justified and allows further analysis of the macroscopic conductance data. Then, for a background conductance of 10 μS cm^{-2} (about 1.2 nS in Fig. 3), which is about three orders of magnitude above the conductance of bare lipid bilayers but still below the resting conductance of the squid giant axon membrane, the mean number of S4–S45 monomers in PC-PE per voltage-dependent conducting aggregate can be estimated to be $N = |V_b|/V_e = 4$ (rounded). The corresponding figure for negatively-charged bilayers is 3 (rounded).

The apparent gating charge, q, of the conducting aggregates can be derived from the V_e parameter through the equation:

$$q = N\, z\, d = (R\, T/\mathfrak{F})/V_e$$

where N is the mean number of peptide monomers forming the channel, $z\,d$ the product of the monomer mobile charge and the fraction of voltage drop (or to a first approximation the fraction of the hydrophobic thickness) the "gate" traverses before achieving activation, R the molar gas constant, T the absolute temperature and $\mathfrak{F}$ Faraday's constant. Here, $q = 3$ in the best cases (S4–S45 in neutral bilayers), but could be as low as 1 (S4 in the same bilayers). Finally, the range of apparent gating charge per monomer (incidentally inversely proportional to $|V_b|$) is 0.8 to 0.5, i.e. quite comparable to values reported for alamethicin (Hall et al. 1984) and zervamicins (Balaram et al. 1992). These apparent gating charges will be compared in the discussion to the ones for native and reconstituted sodium channels.

Single-channel conductances

The single-channel activity induced by S4–S45 was mainly investigated with bilayers formed at the tip of

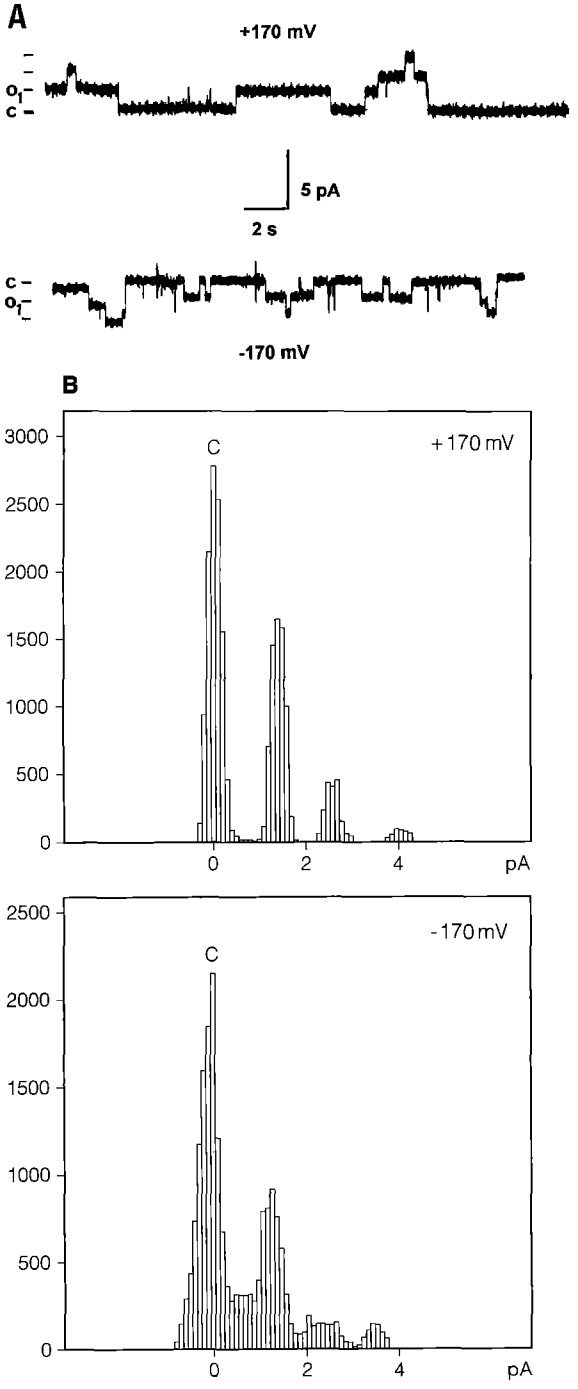

Fig. 5 A, B. Channel activity induced by S4–S45 reconstituted in Montal-Mueller bilayers of reduced area. Peptide aqueous concentration (cis): 10 nM. Lipids: POPC-DOPE (7:3). Aqueous phases: 500 mM NaCl, 10 mM HEPES, pH 7.4. Hole diameter: 70 μm. **A** Recordings and **B** associated histograms at −170 mV and at +170 mV. Data numerically filtered at 150 Hz

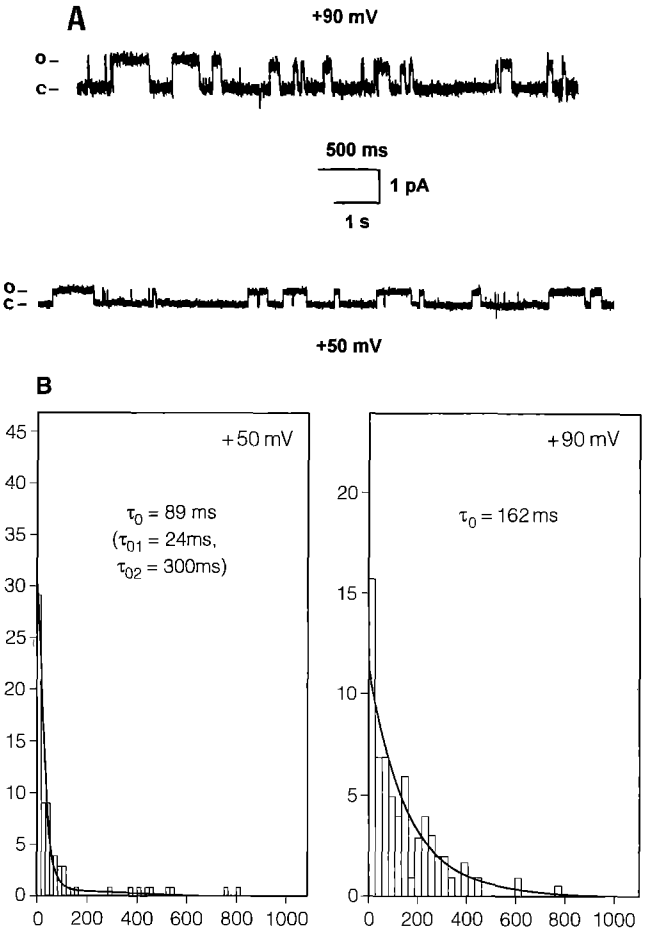

Fig. 6. **A** Single-channel recordings of S4–S45 channels induced in POPC-DOPE (7:3) bilayers at the tip of patch pipettes. Peptide concentration in the bath was 25 nM. Aqueous phases (both sides): 500 mM NaCl, 5 mM HEPES, pH 7.4. Data filtered at 300 and 200 Hz respectively. **B** Associated histograms of channel open lifetimes. The mean open lifetimes appear as τ_0

patch-clamp pipettes but we first proceeded to an "intermediate" configuration, i.e. with Montal-Mueller type bilayers of reduced diameter (75 μm) and formed on a teflon septum whose thickness was also reduced (10 μm).

In neutral planar lipid bilayers. In this configuration and with S4–S45 always in the cis side (aqueous concentration reduced by at least an order of magnitude relative to macroscopic conductance experiments), single-channel events were detected but a high filtering had to be used. Figure 5 A, B show current recordings and associated amplitude histograms taken at both extremes of the voltage range (−170 and +170 mV). There is evidence for multichannels for which the current transitions have the same amplitude (8.4 pS). Qualitatively, positive voltage favours longer open lifetimes and higher probability of opening. Note quite rare sublevels, for example right at the start of the bottom trace.

Figure 6 A shows representative single-channel traces obtained with the patch configuration at two different potentials: +50 and +90 mV. As plotted later (Fig. 8), the conductance amplitude is about 9 pS. The open lifetimes histograms (restricted to activity periods) of Fig. 6 B confirm the voltage-dependence of the mean duration of the open state (89 and 162 ms at +50 and +90 mV respectively) and of the probability of opening (P_0 = 0.40 and 0.60). However, S4–S45 channels failed to reach full activation since P_0 seemed to saturate to 0.70 at higher voltages (+120 and +170 mV). Note that at high negative voltages, the P_0 limit was around 0.35. Although some data is missing below 50 mV, the voltage-depen-

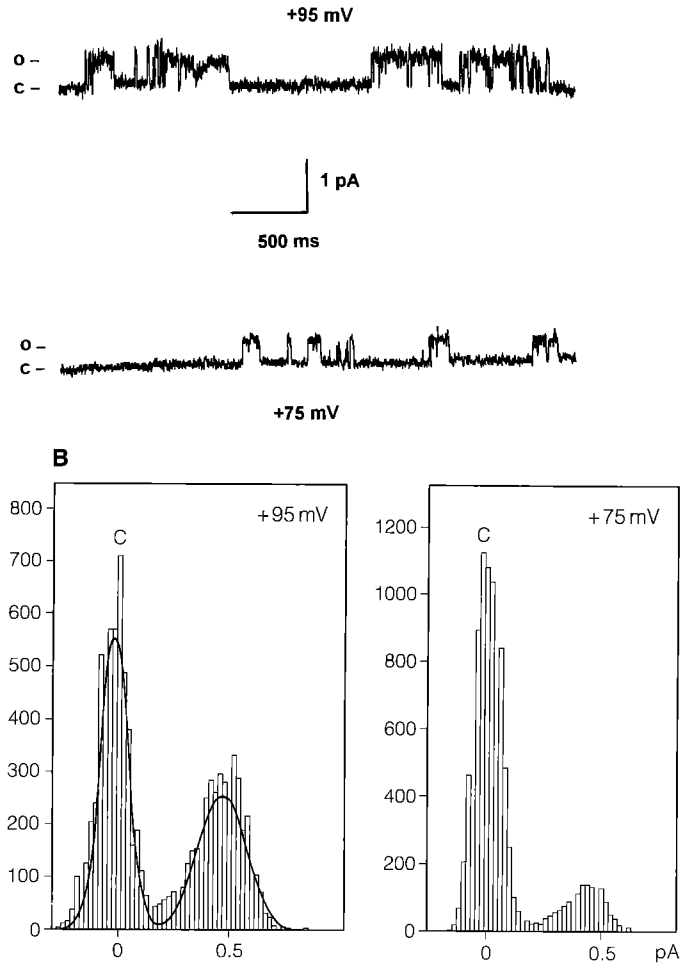

Fig. 7. A Single-channel recordings of S4–S45 channels induced in POPS-DOPE (1:1) bilayers at the tip of patch pipettes. Peptide concentration: 5 nM. During the acquisition, the low-pass filter was set at 900 Hz. Data numerically refiltered at 200 Hz. Gaussian smoothing of amplitude histograms **B** gives a mean conductance of 5.5 pS

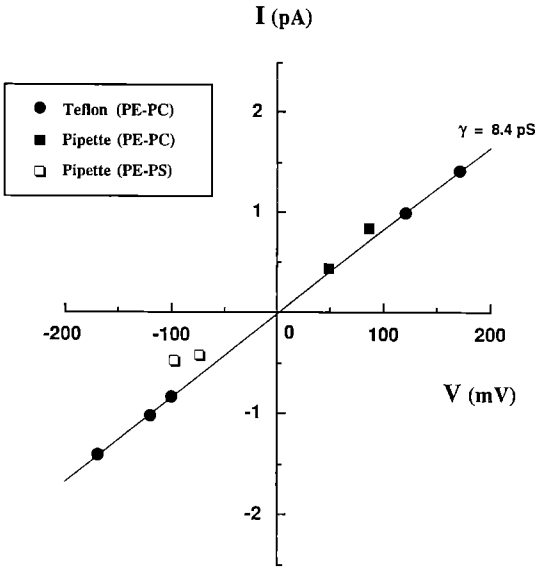

Fig. 8. Current-Voltage relationships of S4–S45 single-channels reconstituted into bilayers formed by the two methods (see insert). Solutions both sides of bilayers: 500 mM NaCl, 10 mM HEPES, pH 7.4. Temperature: 22–24 °C. Only the most frequently observed events are pooled here. For neutral bilayers formed on teflon septa, the slope conductance is 8.4 pS (*solid line*)

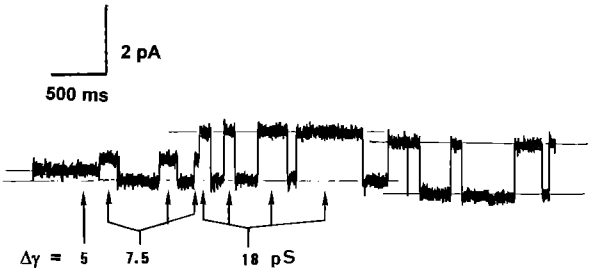

Fig. 9. Transitions between conductance levels. Single-channel recording of S4–S45 channels in pipette-supported POPS-DOPE (1:1) bilayers at +75 mV. Upward deflections correspond to channel opening. Peptide concentration: 5 nM. Low-pass filter frequency: 1 kHz. Data numerically refiltered at 200 Hz

dence of P_0 (voltage increment resulting in an *e*-fold change in P_0) was in the 9–25 mV range and compatible with the macroscopic conductance results where V_e lies between 9 and 19 mV in the same (neutral) lipid system.

In negatively-charged lipid bilayers. With these bilayers, the same conductance of 8–9 pS was also found but it turned out that the most probable single-channel conductance was about 5–6 pS as illustrated with traces at +75 and +95 mV in Fig. 7A. Note faster events in this lipid mixture, the flickering pattern and the longer duration of bursts at the higher potential. The probability of opening was still increased at the higher voltage (see the associated amplitude histograms, Fig. 7B) but it remained more modest than in neutral bilayers at equivalent voltages. With PS-containing bilayers, P_0 was only 0.20 and 0.45 at +75 mV and +95 mV respectively, as if the activation curve was shifted to the right. This is consistent with macroscopic conductance experiments where (other parameters being equivalent) negatively-charged bilayers did not develop (and tolerate!) a current density as high as neutral bilayers did. Accordingly, the reference conductance used to define characteristic voltages V_c was 5 nS for PS-PE bilayers instead of 50 nS for PC-PE ones.

The single-channel conductance data for the most probable events are summarized in an I–V plot (Fig. 8). A linear regression through the points obtained from neutral bilayers formed on teflon septa yields a slope conductance equal to 8.4 pS. By comparison, the unit conductance is not significantly different for tip-dip bilayers of the same lipid composition but seems smaller for negatively-charged tip-dip bilayers (about 5 pS). Other and larger conductance levels, correlated with leakier membranes, were occasionally observed (especially when bilayers were reformed at the tip of pipettes) roughly of 15, 20, 40 and 80 pS. More rarely, fluctuations between different conductance levels could be detected as illustrated with the trace of Fig. 9. Three levels at about 5 pS, 7.5 pS and 18 pS can be identified with some transitions occurring on top of smaller ones.

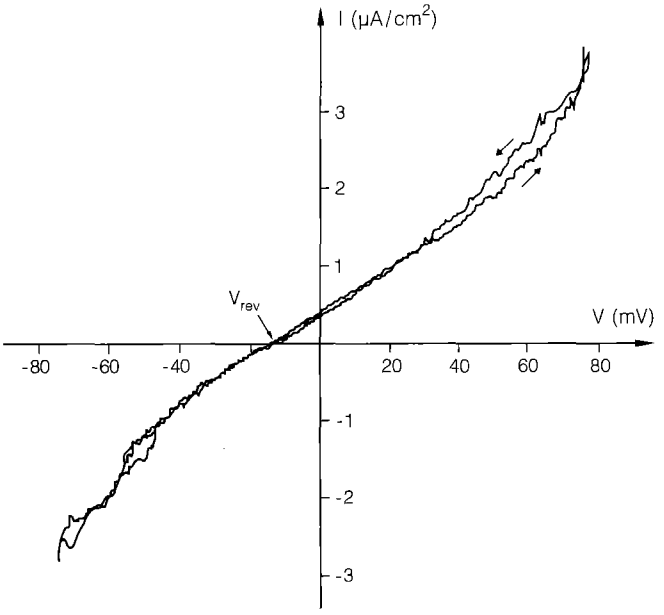

Fig. 10. Ionic selectivity at the macroscopic level under ionic gradients. I–V plot of a Montal-Mueller POPS-DOPE (1:1) bilayer doped with S4–S45 peptide (450 nM). Aqueous phases: 500 mM NaCl (cis)/450 mM KCl + 50 mM NaCl (trans). Period of the voltage triangular wave: 80 s. V_{rev} is −14 mV

Ionic selectivity

Experiments were undertaken to determine the ionic selectivity of S4–S45 channels. I–V curves recorded at the beginning of macroscopic conductance experiments under asymmetric ionic conditions (500 mM NaCl/450 mM KCl + 50 mM NaCl: cis/trans) showed reversal potentials averaging −14 mV (for example, see Fig. 10). The application of the Goldman-Hodgkin-Katz equation yields $P_{Na}/P_K = 3.0$, the cationic/anionic permeability ratio (P_{Na}/P_{Cl}) having been estimated to be 2.5 in previous independent experiments. Later on, zero-current voltages shifted progressively towards the origin as the background or leak conductance increases. In order to settle this point, a few experiments were performed at the single-channel level with patch-bilayers formed between asymmetric solutions and submitted to voltage ramps (amplitude 100 mV, period 80 s). Both background and single-channel currents reversed at the same potential (about −12 mV). Given the K–Na gradients and still assuming P_{Na}/P_{Cl} of 2.5, a ratio $P_{Na}/P_K = 3.1$ could be estimated.

Discussion

With the aim of testing the potential involvement of S45 in the gating or in the permeation pathway of voltage-dependent sodium channels, a 34-mer peptide mimicking the S4–S45 fragment was synthesized. This peptide displays interesting functional features but before comparing them to native or reconstituted sodium channels and to other peptides modelling aspects of those channels, we first discuss the peptide conformation in the light of current models.

The conformation of a related S4 sequence (from the first domain of rat brain I and II sodium channels) was studied by high resolution proton NMR (Mulvey et al. 1989) and found to be α-helical up to I_{14} (tentatively corresponding to L_{15} in our peptide) in deuterated trifluoroethanol/water (9:1). If S4 were mainly α-helical in the membrane during activation, then a pore made up of the juxtaposition of hydrophilic sectors of more or less parallel rods cannot be clearly defined and the best candidate for pore lining with the present peptide would intuitively be the S45 part. Indeed, the helical wheel projection of S45 does reveal a hydrophilic sector (due to T_{26} and S_{34} although slightly perturbed by A_{30}). Quantitatively, both the average hydrophobicity $\langle H \rangle$ and hydrophobic moment $\langle \mu_H \rangle$ (using Eisenberg's (1984) hydropathy scale) are higher for S45 (residues 23–34): +0.51, +0.25 respectively, than for S4 (residues 1–22): −0.11, +0.11.

Our circular dichroism determination of S4–S45 secondary structure cannot discriminate between either Guy and Conti's (1990) or Durell and Guy's (1992) models. Within experimental errors, the 45% helical conformation (i.e. fifteen residues), found as the mean for the two lipid systems we assayed, do not conflict with the former model. Indeed Guy and Conti (1990) assumed that only the middle portion of S4 (S4 h: 8 residues) would be helical at rest. This would allow 7 out of 12 residues in S45 to be in the helical conformation. On the other hand, the averaged β-content of S4–S45 in lipids (8 residues) could represent the "flexible region" between both segments which was hypothesized in the latter model (Durell and Guy 1992). However, no direct inferences as to the actual peptide conformation in the channel activated state can be drawn from these CD experiments. For the time being, a 3_{10} helical "active" conformation, as postulated by Sato and Matsumoto (1992), which would align arginine residues in the pore lumen cannot be excluded.

In macroscopic conductance experiments, the peculiar shape of I–V curves (crossing of ascending and falling limbs) points to a recruitment of voltage-dependent and "right-sized" conducting aggregates with positive voltage which are then somehow locked into large ohmic pores (Boheim and Kolb 1978) on return to rest. Conversely, sweeping back from high negative voltage deactivate the leaky component. The symmetry of I–V curves may result from a more or less even partitioning of S4–S45 between both (cis/trans) bilayer interfaces presumably favoured by the increased length and mean hydrophobicity of S4–S45 as compared to S4. The latter (from Tosteson) was also found to induce more symmetrical I–V curves, in our hands, than previously reported (Tosteson et al. 1988). Apart from the slightly different lipid mixtures used for planar bilayer formation, this discrepancy might be due to the free terminals of Tosteson's peptide while the present S4–S45 was C-amidated and N-acetylated.

The sequence of normalized unit conductances in Fig. 9 (1:1.5:3.6) contrasts with the alamethicin one (1:4.6:9.6 or 1:15:68, restricted to the first three sublevels and whether or not the lowest level of 19 pS is taken into account, Hanke and Boheim 1980). Thus, the dynamic "barrel-stave" model of pores of varying diameters and accounting for the sublevels by the uptake and release of

monomers into conducting aggregates (Baumann and Mueller 1974) seems to be excluded here. A straightforward application of formulas yielding pore diameter and conductance from simple geometrical considerations (cylindrical pore delimited by helical rods, see Sansom 1991) would only give the actual range of observed conductances if the conductivity inside the pore were 1/40 the bulk value, implying an energy barrier of about 3.5 kT. Rather than the fluctuating "barrel-stave" situation, the S4–S45 behaviour evokes partially coupled parallel channels of fixed sizes (multiples of 5 and 8 pS units tentatively assigned to bundles of 3 and 4 monomers) as recently modelled by Berry and Edmonds (1993).

Whatever the peptide assayed (S4 or S4–S45), macroscopic currents in negatively-charged bilayers are, for a given voltage, one magnitude smaller than in neutral bilayers. However, application of the Gouy-Chapman-Stern theory (with $K_{Na} = 0.2\ M^{-1}$) would point to a 5-fold increase of sodium ion concentration at the charged bilayers surface. Besides, Fluorescence Energy Transfer experiments in vesicles with a NBD-labelled S4 (Rapaport et al. 1992) and adsorption experiments with poly-Lys or poly-Arg (Kim et al. 1991) argue for a strong binding of these peptides on acidic bilayers. The high density of positive charges at the mouth of the S4–S5 aggregates might well locally reverse the expected negative surface potential. Furthermore, interfacial electrostatic interactions between PS head groups and the numerous arginines in S4–S45, not only favour some peptide structuration, as shown by the CD data, but are likely to restrict voltage-driven transmembrane location of the peptide. Presumably, at rest, there are peptide pre-aggregates lying flat on the bilayer with the S45 region partly buried in the hydrophobic core.

The amount of displaced charge reported here remains modest, but still quite comparable to electrophysiological data where it amounts to from 3–4 (Vandenberg and Bezanilla 1991) to 7 elementary charges (Conti and Stühmer 1989) for the activation process and, as recently estimated, to 1.2 (Greef and Forster 1991) for inactivation. It should be mentioned that for batrachotoxin-modified (inactivation removed) and purified sodium channels reconstituted into lipid bilayers, the figure is between 1 and 4 (Recio-Pinto et al. 1990; Behrens et al. 1989). In our view and although counter-charges (negative) available on the other segments and whose opposite movement remains possible were not taken into account, an apparent gating charge of 2–3 as suggested by the present study (whether 3 or 4 monomers are considered) would rather imply a "helical screw" mechanism of limited amplitude. On the other hand, the effects of site-specific antibodies raised against different parts of S4 seem to support a large movement of S4 segments within the whole channel during the gating (Kra-Oz et al. 1992).

Table 2 compares the main functional properties of synthetic peptides designed to model voltage-sensitive sodium channels. It is clear from the outset that these peptides only partially account for the essential features of native channels. Nevertheless, S4–S45 compares favourably with the other peptides. The most probable single-channel conductance induced by S4–S45 peptide (5 or 8 pS) is significantly smaller than those reported by Tosteson (70 pS and other higher levels) for S4 alone and more in line with electrophysiological data, especially with reconstituted batrachotoxin-modified channels (Recio-Pinto et al. 1990; Bendahhou et al. 1991). As regards selectivity, one should not infer cationic or anionic permeability from the sign of the charged residues supposed to line the lumen. A number of basic peptides, for example mastoparan (Mellor and Sansom 1990), were shown to be cation-selective in neutral bilayers. Either the positive residues would be screened by anions, allowing the permeation of cations, or else the predominant energy barrier would not be at the level of a basic residue. The selectivity for sodium over potassium ions in purified and reconstituted voltage-dependent sodium channels ranges from 2.5–4.0 in BTX-modified preparations (Castillo et al. 1992; Behrens et al. 1989) up to 7 with untreated channels during pulses (Rosenberg et al. 1984). These figures and our results have to be compared with P_{Na}/P_K from native sodium channels in excitable membranes, which amounts to about 12 in the squid giant axon for instance (Chandler and Meves 1965).

To conclude, not only does the inclusion of S45 not impede the intrinsic S4 voltage-dependence but both the reduced single-channel conductance and the increased selectivity of S4–S45 for sodium argue for a diameter restriction brought about by the S45 fragment in the open configuration. This study thus argues for a functional implication of S45 in the inner part of the permeation pathway as postulated by molecular modelling (Durell and Guy 1992), S45 being drawn inwards as S4 becomes exposed outside. Obviously, the in situ conformation of S4–S45, being constrained by the whole protein folding,

Table 2. Comparison between synthetic peptides modelling the voltage-sensitive sodium channel

Segment (Domain)	Type	A.a.[a] (+, −)	Lipids	V_e (mV)	γ (pS)[b]	P_{Na}/P_K	Ref.
S3 (I)	Rat brain I	22 (0, 4)	Zwitt.	(∞)	20 (5–60)	1.0	Oiki et al. (1988b)
S4 (IV)	*E. electricus*	22 (8, 0)	Negat.	10	70, 300, 500	0.8	Tosteson et al. (1989)
S4–S45(IV)	*E. electricus*	34 (8, 0)	Negat.	15–35	5.5 (8, 15, 20)	3.0	This study
S4–S45	*E. electricus*	34 (8, 0)	Zwitt.	10–20	8.5 (20, 40, 80)	ND[c]	This study
S6 (I)	Rat brain I	22 (0, 0)	?	?	No channels	?	Montal (1990)

[a] Number of total amino acids with basic and acidic residues in brackets
[b] Values in bold correspond to the most probable conductances in NaCl 500 mM solutions
[c] Not determined

is likely to be different from the isolated peptide and we do not believe that the S45 region of the fourth domain is the only constituent of the sodium channel selectivity filter. A further and more realistic polypeptide model should include the SS1-SS2 region linked to S4–S45. Likewise, it might prove valuable to assay S4–S45 from other domains, in particular the one from domain II which contains a proline in the centre. Although the present work confirms that this residue is not essential for an appreciable voltage-sensitivity (see also Duclohier et al. 1992), how would a resulting helix kink in one of the segments influence the voltage-dependence of the whole assembly? S4 (domain II) also presents next to this Pro the only Trp of all the S4–S45 fragments. Since each SS1–SS2 segment is endowed with 1 or 2 Trp, a photodeactivation study with those model peptides in planar lipid bilayers should discriminate which Trp is most responsible for the effect reported on sodium channels in squid giant axons (Conti et al. 1988). No doubt, the strategy using model peptides fostered by the latest developments in automatic peptide synthesis will be further extended and ever more complement mutagenesis and cDNA expression investigations of structure-function relationships in ionic channels.

Acknowledgements. We are grateful to Dr. M. T. Tosteson (Harvard University) for kindly supplying to us a sample of S4. We also thank Dr. A. Van Dorsselaer (Neurochimie, Strasbourg University) for FAB mass characterization, M. El Hajji (Sanofi, Notre-Dame-de-Bondeville, France) for peptide sequencing, L. Brachais (URA 500) for circular dichroism measurements, Dr. G. Spach (URA 500) for his support and M. S. P. Sansom (Oxford University) for helpful discussions. This work was supported by GDR 0964 CNRS "Canaux peptidiques". M. B. also acknowledges the CRSNG (Canada) for a postdoctoral fellowship.

References

Balaram P, Krishna K, Sukumar M, Mellor IR, Sansom MSP (1992) The properties of ion channels formed by zervamicins. Eur Biophys J 21:117–128

Baumann G, Mueller P (1974) A molecular model of membrane excitability. J Supramolec Struc 2:538–557

Behrens MI, Oberhauser A, Bezanilla F, Latorre R (1989) Batrachotoxin-modified sodium channels from squid optic nerve in planar bilayers: ion conduction and gating properties. J Gen Physiol 93:23–41

Ben-Efraïm I, Bach D, Shai Y (1993) Spectroscopic and functional characterization of the putative transmembrane segment of the minK potassium channel. Biochemistry 32:2371–2377

Bendahhou S, Thoiron B, Duclohier H (1991) Purification of sodium channel from squid mantle and reincorporation into planar lipid bilayers. CR Acad Sci Paris t 312 Sér III:277–284

Berry RM, Edmonds DT (1993) Correlated ion flux through parallel pores: application to channel subconductance states. J Membr Biol 133:77–84

Boheim G, Kolb HA (1978) Analysis of the multi-pore system of alamethicin in a lipid membrane: I. Voltage-jump current relaxation measurements. J Membr Biol 38:99–150

Brahms S, Brahms J (1980) Determination of protein secondary structure in solution by vacuum ultraviolet circular dichroism. J Mol Biol 138:149–178

Brullemans M, Tancrède P (1987) Influence of torus on the capacitance of asymmetrical phospholipid bilayers. Biophys Chem 27:225–231

Castillo C, Villegas R, Recio-Pinto E (1992) Alkaloid-modified sodium channels from lobster walking leg nerves in planar lipid bilayers. J Gen Physiol 99:897–930

Catterall WA (1986) Voltage-dependent gating of sodium channels correlating structure and function. Trends Neurosci 9:7–10

Chandler WK, Meves H (1965) Voltage-clamp experiments on internally perfused giant axons. J Physiol (London) 180:788–820

Chang CT, Wu CSC, Yang JT (1978) Circular dichroic analysis of protein conformation: inclusion of the β-turns. Anal Biochem 91:13–31

Conti F, Stühmer W (1989) Quantal charge redistributions accompanying the structural transitions of sodium channels. Eur Biophys J 17:53–59

Conti F, Cantú AM, Duclohier H (1988) Orientation of the tryptophans responsible for the photoinactivation of nerve sodium channels. Eur Biophys J 16:73–81

Duclohier H, Molle G, Dugast JY, Spach G (1992) Prolines are not essential residues in the "barrel-stave" model for ion channels induced by alamethicin analogues. Biophys J 63:868–873

Durell SR, Guy HR (1992) Atomic scale structure and functional models of voltage-gated potassium channels. Biophys J 62:238–250

Eisenberg D (1984) Three-dimensional structures of membrane and surface proteins. Annu Rev Biochem 53:595–623

Greef NG, Forster IC (1991) The quantal gating charge of sodium channel inactivation. Eur Biophys J 20:165–176

Guy HR, Conti F (1990) Pursuing the structure and function of voltage-gated channels. Trends Neurosci 13:201–206

Hall JE, Vodyanoy I, Balasubramanian TM, Marshall GR (1984) Alamethicin: a rich model for channel behavior. Biophys J 45:233–247

Hanke W, Boheim G (1980) The lowest conductance state of the alamethicin pore. Biochim Biophys Acta 596:456–462

Hanke W, Methfessel C, Wilmsen HU, Boheim G (1984) Ion channel reconstitution into planar lipid bilayers on glass pipettes. Biochem Bioenerg J 12:329–339

Isacoff EY, Jan YN, Jan LY (1991) Putative receptor for the cytoplasmic inactivation gate in the Shaker K^+ channel. Nature 353:86–90

Keynes RD (1992) A new look at the mechanism of activation and inactivation of voltage-gated ion channels. Proc R Soc London Ser B 249:107–112

Keynes RD, Greef NG, Forster IC (1990) Kinetic analysis of the sodium gating current in the squid giant axon. Proc R Soc London Ser B 240:411–423

Kim J, Mosior M, Chung LA, Wu H, McLaughlin S (1991) Binding of peptides with basic residues to membrane containing acidic phospholipids. Biophys J 60:135–148

Kra-Oz Z, Spira G, Palti Y, Meiri H (1992) Involvement of different S4 parts in the voltage dependency of Na channel gating. J Membr Biol 129:189–198

Langosch D, Hartung K, Grell E, Bamberg E, Betz H (1991) Ion channel formation by synthetic transmembrane segments of the inhibitory glycine receptor: a model study. Biochim Biophys Acta 1063:36–44

Lear JD, Wasserman ZR, DeGrado WF (1988) Synthetic amphiphilic peptide models for protein ion channels. Science 240:1177–1181

Mellor IR, Sansom MSP (1990) Ion-channel properties of mastoparan, a 14-residue peptide from wasp venom, and of MP3, a 12-residue analogue. Proc R Soc London Ser B 239:383–400

Merrifield RB (1963) Solid phase peptide synthesis: I The synthesis of a tetrapeptide. J Am Chem Soc 89:2149–2154

Molle G, Dugast JY, Duclohier H, Daumas P, Heitz F, Spach G (1988) Ionophore properties of a synthetic alpha-helical transmembrane fragment of the mitochondrial H^+ ATP synthetase of *Saccharomyces cerevisiae*: comparison with alamethicin. Biophys J 53:193–203

Montal M (1990) Channel protein engineering: an approach to the identification of molecular determinants of function in voltage-

gated and ligand-regulated channel proteins. In: Narahashi N (ed) Ion channels. vol 2. Plenum Press, New York, pp 1–31

Montal M, Mueller P (1972) Formation of bimolecular membranes from lipid monolayers and a study of their electrical properties. Proc Natl Acad Sci, USA 69:3561–3566

Mueller P, Rudin DO (1968) Action potentials induced in biomolecular lipid membranes. Nature 217:713–719

Mulvey D, King GF, Cooke RM, Doak DG, Harvey TS, Campbell ID (1989) High resolution ^{1}H NMR study of the solution structure of the S4 segment of the sodium channel protein. FEBS Lett 257:113–117

Noda M, Shimizu S, Tanabe T, Takai T, Kayano T, Ikeda T, Takahashi H, Nakayama H, Kanaoka Y, Minamino N, Kangawa K, Matsuo H, Raftery MA, Hirose T, Inayama S, Hayashida H, Miyata T, Numa S (1984) Primary structure of *Electrophorus electricus* sodium channel deduced from cDNA sequence. Nature 312:121–127

Oiki S, Danho W, Madison V, Montal M (1988 a) M2 δ: a candidate for the structure lining the ionic channel of the nicotinic cholinergic receptor. Proc Natl Acad Sci, USA 85:8703–8707

Oiki S, Danho W, Montal M (1988 b) Channel protein engineering: synthetic 22-mer peptide from the primary structure of the voltage-sensitive sodium channel forms ionic channels in lipid bilayers. Proc Natl Acad Sci, USA 85:2393–2397

Patlak J (1991) Molecular kinetics of voltage-dependent Na^+ channels. Physiol Rev 71:1047–1080

Pawlak M, Stankowski S, Schwarz G (1991) Mellitin-induced voltage-dependent conductance in DOPC lipid bilayers. Biochim Biophys Acta 1062:94–102

Rapaport D, Danin M, Gazit E, Shai Y (1992) Membrane interactions of the sodium channel S4 segment and its fluorescently-labeled analogues. Biochemistry 31:8868–8875

Rayner MD, Starkus JG, Ruben PC, Alicata DA (1992) Voltage-sensitive and solvent-sensitive processes in ion channel gating: kinetic effects of hyperosmolar media on activation and deactivation of sodium channels. Biophys J 61:96–108

Recio-Pinto E, Thornhill WB, Duch DS, Levinson SR, Urban BW (1990) Neuraminidase treatment modifies the function of electroplax sodium channels in planar lipid bilayers. Neuron 5:675–684

Rosenberg RL, Tomiko SA, Agnew WS (1984) Single-channel properties of the reconstituted voltage-regulated Na channel isolated from the electroplax of *Electrophorus electricus*. Proc Natl Acad Sci USA 81:5594–5598

Sansom MSP (1991) The biophysics of peptide models of ion channels. Prog Biophys Molec Biol 55:139–235

Sato C, Matsumoto G (1992) Proposed tertiary structure of the sodium channel. Biochem Biophys Res Commun 186:1158–1167

Schauf CL, Bullock JO (1980) Solvent substitution as a probe of channel gating in *Myxicola*: differential effects of D_2O on some components of membrane conductance. Biophys J 30:295–306

Slesinger PA, Jan YN, Jan LY (1993) The S4–S5 cytoplasmic loop forms part of the inner mouth of the *Shaker* potassium channel. Biophys J 64 (2,2):A114

Smith-Maxwell CJ, Kanevsky M, Aldrich RW (1993) Potassium channel activation can be slowed down by mutations in the S4 and S4–S45 linker regions. Biophys J 64 (2,2):A200

Spach G, Duclohier H, Molle G, Valleton JM (1989) Structure and supramolecular architecture of membrane channel-forming peptides. Biochimie 71:11–21

Stühmer W (1991) Structure-function studies of voltage-gated ion channels. Annu Rev Biophys Chem 20:65–78

Stühmer W, Conti F, Suzuki H, Wang X, Noda M, Yahagi N, Kubo N, Numa S (1989) Structural parts involved in activation and inactivation of the sodium channel. Nature 339:597–603

Tosteson MT, Auld DS, Tosteson DC (1989) Voltage-gated channels formed in lipid bilayers by a positively charged segment of the Na-channel polypeptide. Proc Natl Acad Sci, USA 86:707–710

Vandenberg CA, Bezanilla F (1991) Single-channel, macroscopic and gating currents from sodium channels in the squid giant axon. Biophys J 60:1499–1510

Yool AJ, Schwarz TL (1991) Alteration of ionic selectivity of a K^+ channel by mutation of the H5 region. Nature 349:700–704